From Submicrosecond- to Nanosecond-Pulsed Atmospheric-Pressure Plasmas

Felipe Iza, *Member, IEEE*, James L. Walsh, and Michael G. Kong, *Senior Member, IEEE*

(Invited Paper)

***Abstract*—We have developed a time-hybrid computational model to study pulsed atmospheric-pressure discharges and compared simulation results with experimental data. Experimental and computational results indicate that increasing the applied voltage results in faster ignition of the discharge and an increase in the mean electron energy, opening the door to tunable plasma chemistry by means of pulse shaping. Above a critical electric field of $\sim$2 kV/mm for $\sim$1-mm discharges, pulsed plasmas ignite right after the application of an externally applied voltage pulse. Despite the large pd value (30–300 torr $\cdot$ cm) and the high applied electric field, the discharges are found to be streamer free in a desirable glowlike mode. The comparison of the time evolution of the mean electron kinetic energy as a function of the pulse rise time suggests that a fast rise time is not necessarily the best way of achieving high mean electron energy.**

***Index Terms*—Atmospheric pressure, nanosecond, pulsed plasma, simulation.**

I. Introduction

In THE LAST decade, low-temperature atmospheric-pressure plasmas have opened new venues with potential economic and technological impact in many scientific disciplines. The physics of these discharges, however, remains not fully understood, and the generation of stable yet reactive plasmas continues to attract great attention. Two strategies are commonly used for generating large-scale low-temperature plasmas: 1) arrays of microdischarges in which the increase in surface-to-volume ratio aids to keep the discharges far from thermodynamic equilibrium [1]–[3] and 2) pulsed excitation of the discharges in order to keep them on for times shorter than the time needed for instabilities to develop [4]–[9].

In this paper, we concentrate on the latter and focus on a parallel-plate configuration. This configuration (with and without dielectric barriers) has been used to sustain discharges not only in noble gases (He, Ar) but also in atmospheric air [4]–[8]. By reducing the duration of the discharge down to $\sim$10 ns, instantaneous power in excess of 1 MW/m^2 can be delivered to the system to strike uniform glowlike discharges. Under these conditions, current densities as high as 15 A/cm^2 (typical atmospheric-pressure DBD discharges operate at 10–100 mA/cm^2) can be driven through the discharge, creating a reactive environment, while the gas temperature remains close to room temperature [7]. Our interest focuses on these short-pulsed discharges because they provide an interesting approach not only for generating room-temperature plasmas but also for controlling their chemistry. In this paper, we compare submicrosecond-pulsed (pulse duration of hundreds of nanoseconds) and nanosecond-pulsed (pulse duration of tens of nanoseconds) discharges and highlight differences between the two in terms of their electrical and optical properties. For convenience, we refer to these discharges as short-pulsed atmospheric-pressure plasmas for the remainder of this paper. Despite the high pressure times distance ($pd \sim 30-300$ torr $\cdot$ cm) value and high electric field (approximately kilovolts per millimeter) used to sustain the discharges, the resulting plasmas are filament free as evidenced by single-shot images taken with 5-ns exposure time. These experimental evidences highlight the potential of pulsed short-pulsed atmospheric plasmas as a highly reactive processing tool with well-controlled plasma stability.

Diagnostics of atmospheric-pressure short-pulsed discharges is challenging due to their transient nature and the limited applicability of conventional diagnostic techniques developed for low-pressure plasmas. Therefore, it is difficult to assess quantitatively physical parameters in order to unravel the underpinning principles governing these discharges. Overcoming the experimental difficulties, computer simulations offer a complementary approach. Simulation results can provide insights into the underpinning physical principles and can be used to validate different theories. Two simulation approaches are normally used to study low-temperature plasmas: fluid and particle-in-cell Monte Carlo collision models (PIC-MCC).

Fluid models assume that the electron mean energy can be determined based on the local value of the electric field, an assumption that is not always valid for short-pulsed discharges. In particular, as the pulse duration reduces and its amplitude increases, the applied electric field eventually changes in time and space on the same scale as the electron energy relaxation time (up to several nanoseconds) and length (tens of micrometers) [1]. Therefore, for short-pulsed discharges, a kinetic treatment such as PIC-MCC is needed to capture the electron kinetics accurately. In fact, PIC-MCC models have been used in the past to simulate low-pressure plasmas when the fluid assumptions

Manuscript received October 1, 2008; revised December 11, 2008 and January 27, 2009. First published March 10, 2009; current version published July 9, 2009. This work was supported by the Engineering and Physical Sciences Research Council, U.K. F. Iza also acknowledges the support by the Royal Academy of Engineering, U.K.

The authors are with the Department of Electronic and Electrical Engineering, Loughborough University, LE11 3TU Leicestershire, U.K.

Color versions of one or more of the figures in this paper are available online at http://ieeexplore.ieee.org.

Digital Object Identifier 10.1109/TPS.2009.2014766

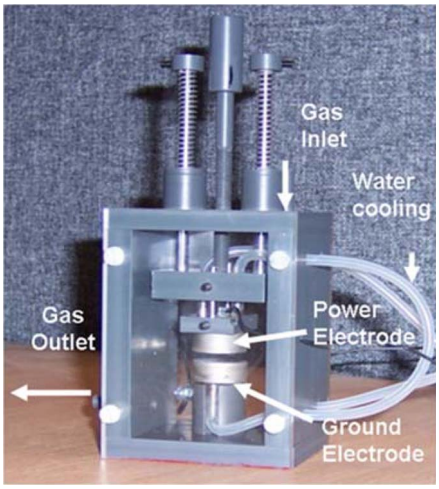

Fig. 1. Experimental setup: Parallel-plate capacitively coupled plasma source with water-cooled stainless-steel electrodes in a Perplex box.

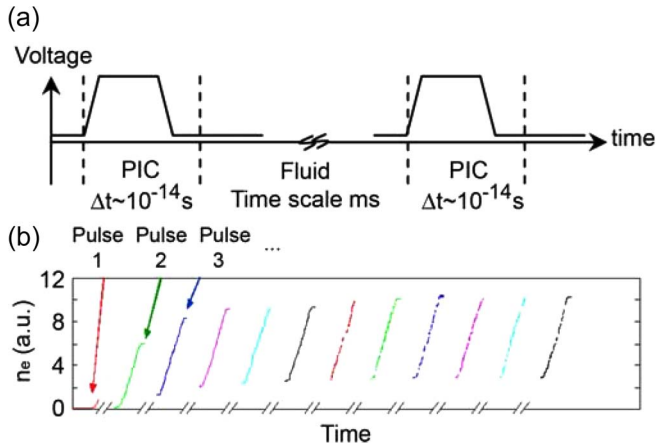

Fig. 2. (a) Schematic representation of the hybrid algorithm. (b) Time evolution of the number of electrons in the PIC-MCC simulation as a function of time. A dynamic steady state is reached after a few pulses.

are not valid [10], [11]. Modeling atmospheric-pressure helium plasmas using a PIC-MCC model, however, requires time steps on the order of $\sim 10^{-14}$ s in order to resolve the high collisionality of the discharge (electron collision frequency $\nu >$ THz) [10], [12]. Since short-pulsed plasmas operate typically with repetition rates on the order of kilohertz and there are clear experimental evidences that each pulse influences the next one (see Fig. 3 and accompanying discussion), reaching a dynamic steady state in a pure PIC-MCC simulation would require computation of $>10^{11}$ time steps, something computationally prohibitive. As a result, PIC-MCC simulation of pulsed discharges is scarce and limited to a single pulse [13].

In this paper, we introduce a hybrid (PIC-MCC + fluid) code that captures particle kinetics during the pulse-on phase of the plasma using a PIC-MCC approach with a time resolution of $\sim$10 fs, and at the same time, it can simulate multiple pulses occurring in time scales of milliseconds by switching to a fluid description during the pulse-off phase. The goal of this code is to support the interpretation of experimental observations, providing a qualitative tool that can be used to validate different hypothesis with regard to the underlying mechanisms that govern these discharges. Although a quantitative agreement between experimental and simulation data would require a more sophisticated model, in its current form, the hybrid model reproduces the main electrical characteristics observed in experiments.

The rest of this paper is organized as follows. A description of the experimental setup and the computational model are presented in Section II. The discharge characteristics of submicrosecond-pulsed discharges are discussed in Section III, and Section IV deals with nanosecond-pulsed discharges. Conclusions are drawn in Section V.

II. Experimental Setup and Computational Model

A. Experimental Setup

The experimental setup used for this paper consists of two parallel stainless-steel disk electrodes, each being 2 cm in diameter (Fig. 1). The electrodes can be water cooled, although this is not required for the experiments presented in this paper as the discharges remain at room temperature. The discharge gap can be varied between 50 μm and 5 mm, and the whole system is housed in a Perspex box. The discharges are sustained in He, which flows into the box at 5 slm. A solid-state pulse generator built in-house is used to deliver high-voltage pulses ranging from 10 ns to 1 μs at repetition rates of up to 20 kHz. The current flowing through the discharge and the voltage across the electrodes are measured with a 200-MHz bandwidth current probe (Pearson Current Monitor 2877), a 250-MHz bandwidth voltage probe (Tektronix P5100), and a digital oscilloscope (Tektronix DPO 4104, 1GHz 5GS/s). An intensified charge-coupled device (iCCD) camera (Andor i-Star DH720) is used to take the images presented in this paper.

B. Simulation Model: Hybrid Approach

Despite their own intrinsic limitations, PIC-MCC and fluid simulations complement each other and can be combined to create a hybrid model for short-pulsed atmospheric-pressure discharges. A PIC-MCC module can provide the kinetic treatment required to model the discharge during the pulse-on phase when the particle kinetics cannot be modeled accurately with the fluid approach. In addition, a fluid module can capture the main discharge physics during the pulse-off phase when the electron mean energy can be reasonably predicted by the local value of the electric field. Therefore, a time-hybrid approach in which the discharge is modeled using alternatively a PIC-MCC technique during the pulse-on phase and a fluid description during the pulse-off phase is a computational efficient approach to capture the physics involved in short-pulsed discharges [Fig. 2(a)]. Switching from the PIC-MCC model to the fluid model can be done soon after the end of the pulse-on phase because at atmospheric pressure, the electron energy relaxation time (approximately nanoseconds) is much shorter than the pulse-off period (approximately microseconds).

PIC-MCC Model: The PIC-MCC code used in this paper is the same code employed in [14] to model atmospheric-pressure RF microdischarges. The code is based on XPDP1 [15], and it has been restructured to speed up the computation. In addition, the weight of the particles [10]–[12], i.e., the number of particles represented by one computer superparticle, dynamically changes to adapt to the large changes in plasma density

expected in short-pulsed atmospheric-pressure plasmas. This procedure ensures that the number of superparticles in the simulation domain remains high and within computationally manageable bounds. The number of superparticles used in this paper is kept in the range of $2 \cdot 10^5 - 5 \cdot 10^5$, and parallel computing is exploited to reduce the computation time.

The PIC-MCC module tracks electrons and He^+ ions individually according to the Newton–Lorentz equation, while the distribution of background neutrals is assumed to be time independent and uniform in space. Elastic, excitation, and ionization electron-neutral collisions are accounted for in the model. For ions, elastic scattering and charge exchange collisions are included. For simplicity and similar to what is normally done in fluid models, a constant ion-induced secondary electron emission coefficient of 0.1 is used in this paper. A more realistic representation of the secondary emission processes accounting for the dependence on the energy of the impinging particle and field emissions [16] will be incorporated in the future.

Fluid Model: During the pulse-off phase, no external voltage is applied to the plasma and the evolution of the discharge is predicted in a first approximation by the solution of the ambipolar diffusion equation. The evolution of the density profile in terms of harmonic modes is [17]

$$n(x,t) = \sum A_i \exp\left(-\frac{t}{\tau_i}\right) \cos\left(\frac{(2i+1)\pi x}{L}\right) \qquad (1)$$

where $n(x,t)$ is the plasma density, A_i and $\tau_i \approx (1/T_e\mu_i)(L/(2i+1)\pi)^2$ are the amplitude and the decay time constant of the ith mode, respectively, L is the discharge gap, T_e is the electron temperature, and μ_i is the ion mobility. Upon completion of a pulse-on phase, the plasma is left to relax until the average electron energy is less than 0.75 eV and the plasma potential is less than 5 V. At that time, the PIC-MCC simulation is stopped and a Fourier transform of the density profile is performed to determine the coefficients A_i's. The time is then advanced with the evolution of the plasma being given by (1). The new density profile at the end of the pulse-off phase is then loaded to the PIC-MCC simulation as the initial density for the next pulse simulation. The procedure used to load an arbitrary initial density distribution (profile) in the PIC-MCC simulation is discussed in [10] and [18].

The evolution of the number of electrons in the PIC-MCC simulations as a function of time is shown in Fig. 2(b). Due to the exponential growth of the discharge during its ignition (see Section III-B), the discharge reaches a dynamic steady state over just a few pulses.

In order to improve the agreement between simulation results and experimental data, the diffusion of plasma species during the pulse-off phase ($D \sim T_e\mu_i$) had to be increased to compensate for the loss of charged species by mechanisms other than ambipolar diffusion. In particular, recombination processes play an important role in atmospheric-pressure discharges. Based on the simulation results obtained using fluid models [19], recombination between electrons and He dimer ions is the dominant recombination process and has an initial time constant of ~ 100 μs. In addition, molecular impurities present in the gas further affect the loss rate of electrons during the pulse-off phase in the experiments. An estimation based on relevant reaction rates for oxygen impurities suggests a time constant of 10–100 μs. Although, in the presence of impurities, new electrons can also be incorporated via Penning ionization, experimental results suggest that the net result of recombination, attachment, and Penning ionization is a faster electron loss rate than the one predicted by ambipolar diffusion. An explicit treatment of recombination, attachment, and Penning processes would require additional chemistry to be incorporated in the fluid and PIC-MCC models. At present, these effects are introduced by multiplying the ambipolar diffusion constant by an *ad hoc* correction factor ($\sim$10) until a satisfactory qualitative agreement between simulation results and the experimental current waveform is obtained.

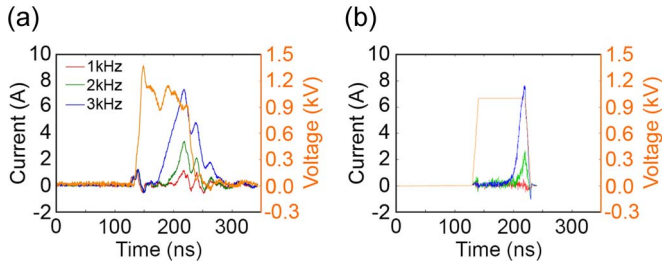

Fig. 3. Voltage and current evolution during a 1-kV 100-ns pulsed discharge. (a) Experimental data and (b) simulation results.

C. Code Validation

In order to gain confidence in the code, the voltage and current obtained in the simulations are compared with those measured experimentally in a 1-mm He atmospheric-pressure discharge sustained by 1-kV 100-ns pulses with a repetition rate of 1–3 kHz. As shown in Fig. 3, the measured discharge current tends to peak well after the applied voltage reaches its peak and the current peak appears to coincide with the fall of the voltage. Simulation results with an idealized trapezoidal voltage waveform [Fig. 3(b)] are able to capture both the time delay of the current pulse and the cooccurrence of the current peak and voltage fall. From the standpoint of capturing the underpinning physics, the simulation reproduces faithfully the experimental observation, albeit qualitatively. A more quantitative comparison accounting for the overshoot and ringing of the applied voltage is possible if the electronics, external circuit, and parasitic elements of the experimental setup are included in the simulation. The goal of our computational code at present, however, is to unravel underpinning physics rather than the quantitative description of a given device. A detailed description of these aspects will be addressed in the future.

As pulses with higher voltage are used to drive the discharge, the instantaneous current reaches higher values and the limitation of the power supply in maintaining the applied voltage becomes noticeable. To reproduce this effect, the simulations incorporate a resistor in series with an ideal power source, allowing for the reduction of the voltage across the electrodes as the current increases (Fig. 4). The self-consistent solution of the PIC-MCC simulation with an external circuit is described in [15].

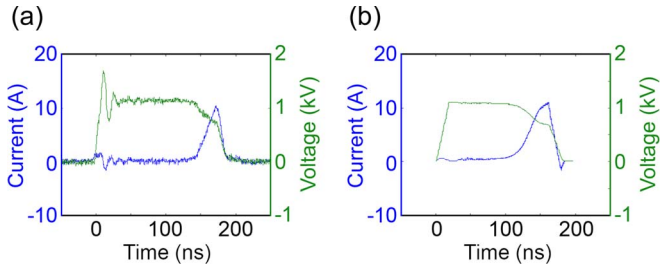

Fig. 4. Current–voltage traces (a) measured and (b) simulated. Note the similarity of the delay between the application of the pulse and the current increase as well as the voltage reduction resulting from the loading of the power supply by the plasma.

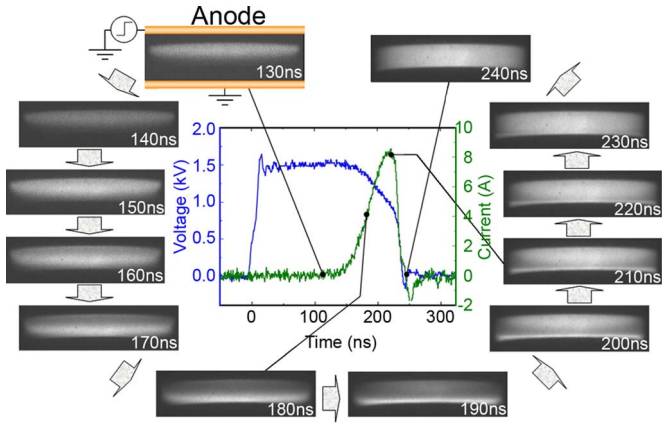

Fig. 5. Evolution of the optical emission from a submicrosecond-pulsed atmospheric-pressure discharge sustained in a 3-mm gap at a repetition rate of 4 kHz. Single-shot images taken with an iCCD camera with a 5-ns exposure time. Images are not calibrated as to unveil the emission profile before the formation of the intense discharge at ∼210 ns.

Although the plasma rig used to obtain the experimental data shown in Fig. 4 is the same as the one used to obtain the data of Fig. 3, the power supply and the wiring setup were improved to minimize parasitic effects. As a result of this improvement and the operation with longer pulses (200 ns in Fig. 4 versus 100 ns in Fig. 3), the waveforms in Fig. 4 are of better quality that those in Fig. 3.

III. Submicrosecond-Pulsed Discharges

A. Emission of a Typical Discharge

In this paper, we distinguish between submicrosecond-pulsed (Section III) and nanosecond-pulsed (Section IV) discharges as we believe that they operate in different regimes. Submicrosecond-pulsed discharges typically last hundreds of nanoseconds, and their current traces have a clear delay with respect to the rising edge of the driving voltage pulse. In these discharges, the electron avalanche initiated by seed electrons from previous pulses [17] is not sufficient to create a plasma dense enough as to perturb the applied electric field. Therefore, secondary electrons are required to create additional avalanches and build up the plasma during each pulse. The typical evolution of the optical emission during one pulse of these discharges is shown in Fig. 5. These images correspond to a 3-mm He atmospheric-pressure plasma driven by 1.5-kV 250-ns pulses with a repetition rate of 4 kHz. The emission starts near the anode and moves gradually toward the cathode as it becomes more intense. After a certain delay of typically ∼100 ns, the discharge current grows sharply and the emission becomes much more intense. In this phase, a bright layer forms near the well-developed cathode sheath and the rest of the discharge remains less emissive. This qualitative description agrees with the one expected from discharges initiated in the Townsend regime and followed by the formation of a cathode-directed ionization front [17], [20].

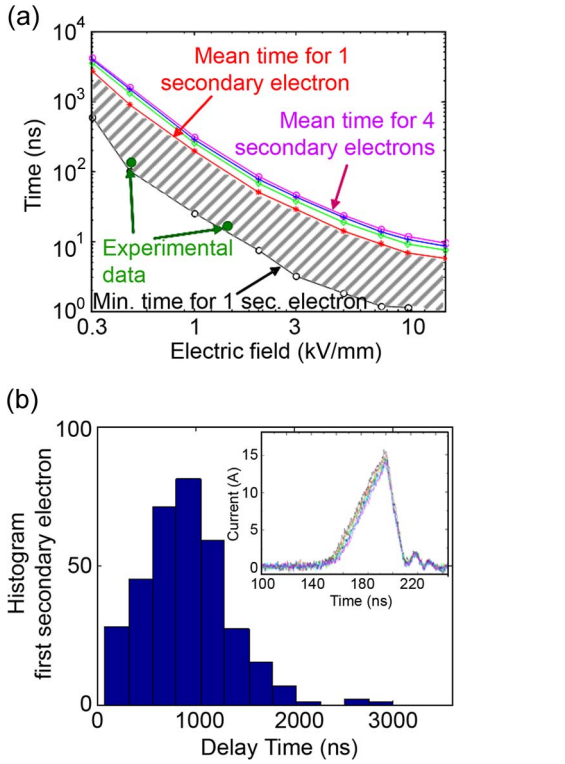

Fig. 6. (a) Time delay for the onset of secondary electron emissions as a function of electric field. (b) Histogram of the delay time for the discharge ignition (as discussed in the text).

B. Discharge Ignition: Experimental Data Versus Simulation Results

The hypothesis of a Townsend discharge during the initial buildup of the plasma can be further probed with PIC-MCC simulations by estimating the delay time for the ignition of the discharge after the voltage pulse is applied. Starting with one electron on the cathode surface that is accelerated toward the anode, the time for the emission of a secondary electron is measured using a PIC-MCC scheme. The process is repeated 10^5 times in order to get meaningful statistical results. The average delay time for the emission of a secondary electron as a function of the applied electric field is shown in Fig. 6. It is noted that the delay for the emission of subsequent electrons is much shorter, and therefore, the emission of the first secondary electron can be taken as an estimation of the discharge ignition delay. As the electric field increases, the delay time for the emission of a secondary electron decreases due to the faster acceleration of electrons and ions in the discharge gap.

While the trend of the delay time as a function of the applied electric field agrees qualitatively with experimental observations, two significant discrepancies can be pointed out.

The first one is the fact that the histogram of the delay time obtained for a given electric field has a broad distribution [Fig. 6(b)], suggesting that pulses will have a markedly different ignition delay. This phenomenon, however, is not observed in experiments. As shown in the inset of Fig. 6(b), the current waveforms of different pulses overlay with each other (the slight difference observed in the experimental curves is actually a drift in time rather than a statistical variation). Second, when the actual delay time observed in experiments is compared with the mean delay obtained in the simulations, it is observed that, experimentally, the ignition takes place approximately an order of magnitude faster.

We believe that these discrepancies are due to the "memory effect" in between pulses. As a result of the discharge ignited in previous pulses, a relatively large number of electrons and ions exist within the discharge gap when a pulse is applied. Each electron and ion can potentially ignite the discharge, each with a statistical time delay similar to the one shown in Fig. 6. However, since the number of seed particles is large and the breakdown takes place soon after the first secondary electrons is emitted, the statistical distribution for the ignition delay time shifts toward shorter times. In fact, a better agreement is found between the minimum delay time observed in the simulation results and the experimentally measured ignition delay (Fig. 6). This "memory effect" also agrees with the results shown in Fig. 3, where an increase in the pulse repetition rate shortens the ignition delay. Therefore, it is concluded that submicrosecond-pulsed plasmas are initiated in the Townsend regime and that secondary electrons are needed to build up the discharge. The delay associated with the time needed for secondary electrons to be created suggests that a "memory effect" from previous pulses needs to be taken into account. It is worth noting that since bare electrodes are used in this paper, the memory effect is due to remaining particles within the gap space and not to charges accumulated on dielectric surfaces. The role of surface charges on dielectric surfaces, when present, is also known to play an important role [4].

C. Time Evolution of the Mean Kinetic Energy

The time evolution of the mean electron energy during a pulse is shown in Fig. 7(a). The mean electron energy increases rapidly as soon as the voltage is applied, reaching close to ~10 eV. This is significantly higher than the mean electron energy observed in discharges that are sustained with continuous excitation (typical electron temperature for continuous excitation ~1 eV [14], [21], [22]). Soon after the initial increase, the mean electron energy starts to drop as a result of the loss of energetic electrons to the anode [Fig. 7(b)] and the formation of a quasi-neutral plasma within the discharge. This quasi-neutral region forms when the space charge starts perturbing the applied electric field. As a result of this perturbation, the electric field across the cathode sheath is enhanced, while that in the quasi-neutral region decreases rapidly. After ~100 ns, the mean energy starts to increase again due to the onset of avalanches across the cathode sheath initiated by secondary electrons. Finally, as the pulse terminates, the electron energy decreases rapidly due to the high collisionality of the plasma.

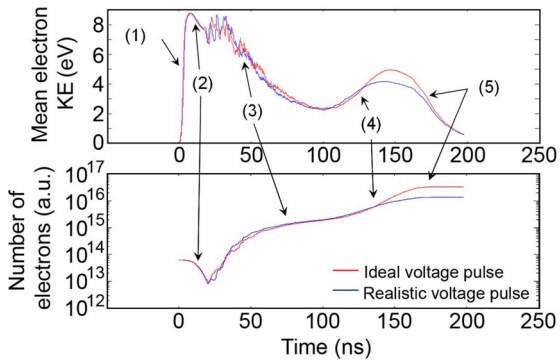

Fig. 7. Generic evolution of (a) the space-average mean electron energy and (b) total number of electrons during a 150-ns pulsed discharge. Simulation results with an ideal voltage source capable of maintaining a constant voltage during the whole duration of the pulse and a real source that gets loaded by the plasma. (1) Avalanche of seed electrons that remain from the previous pulse. (2) Loss of energetic electrons to the anode. (3) Quasi-neutral plasma formation, confinement of low energy electrons. (4) New avalanches initiated by secondary electrons. (5) Pulse end.

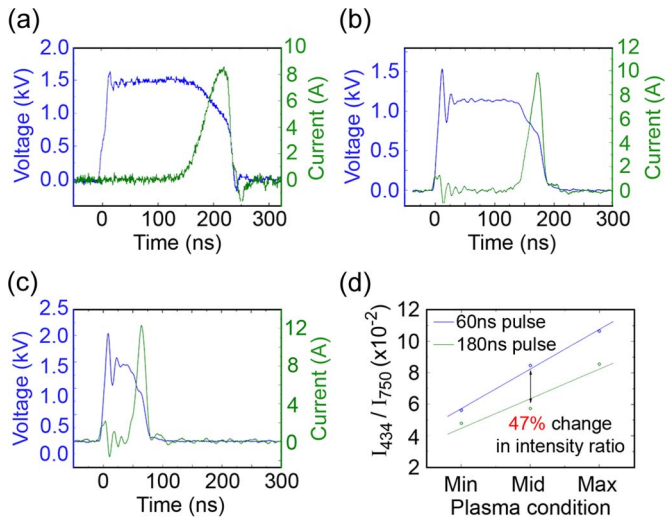

Fig. 8. Experimental voltage–current waveforms of three submicrosecond-pulsed discharges sustained with an average electric field (applied voltage/gap) of (a) 0.5 kV/mm (1.5 kV, 3-mm gap), (b) 0.9 kV/mm (1.1 kV/1.2 mm), and (c) 1.2 kV/mm (1.5 kV/1.2 mm). (d) Argon line intensity ratio 434 nm/750 nm in 60-ns and 180-ns pulsed discharges at three input power conditions: immediately after breakdown (min), at the point immediately before streamers appear (max), and the midpoint between the two (mid).

IV. Nanosecond-Pulsed Discharges

A. Potential Benefit of Shorter Pulses

As the applied electric field increases, the discharges can be generated faster, i.e., with shorter ignition delays and therefore with shorter pulses [Fig. 8(a)–(c)]. The interest on shorter pulses, however, is not because of the duration of the discharge itself but rather because of the increase in electron energy that can potentially be achieved. As shown in Fig. 7(a), the electron energy reaches large values only during a small section of the pulse, suggesting that shorter pulses would have a higher average energy. An indirect evidence of this tendency is shown in Fig. 8(d), where the intensity ratio of two argon lines (434 and 750 nm) is compared for plasmas sustained by 180- and 60-ns pulses. Argon emission is present due to the admixture of a small argon trace (< 0.1%) for diagnostic

purposes. The reduction of the pulsewidth from 180 to 60 ns requires a ∼20% increase of the applied voltage. The increase of the 434-nm/750-nm line ratio, however, is 50%. Since the 434- and 750-nm lines are indicators of the number of electrons with energies above 35.3 and 13.5 eV [23], respectively, the increase in the line ratio suggests an increase in the number of energetic electrons in the 60-ns discharge.

B. Instantaneous Discharge Breakdown

As the electric field is increased, the discharges ignite with shorter and shorter delays [Fig. 8(a)–(c)] and the mean electron energy increases. At some point, the applied electric field is strong enough to cause the formation of a quasi-neutral plasma as a result of the acceleration of seed electrons. In this case, secondary electrons do not play a role in the ignition of the discharge and the gas breaks "instantaneously" as soon as the pulse is applied, i.e., there is no delay associated with the need for the generation of secondary electrons. Breakdown without the need of secondary electrons has been known for a long time and is typically observed when Meek's criterion is satisfied [24]. This breakdown mechanism typically results in the formation of streamers, something not desirable from an application point of view. It is noted, however, that in our experiments and with a 5-ns resolution time, no streamers are observed.

A simple theoretical calculation of the electric field required for this instantaneous ignition of the discharge can be derived by solving Poisson's equation, assuming that the ion density profile left by the initial electron avalanche as it transits the discharge gap has an exponential profile and that the electric field at the anode surface $(x = L)$ is ∼0 when the resulting space charge is high enough as to start perturbing the applied electric field

$$\left.\begin{array}{l} \frac{d^2V}{dx^2} = -\frac{q}{\varepsilon_o} n_o \exp(\alpha x) \\ V(0) = 0 \\ \frac{dV}{dx}\big|_L = 0. \end{array}\right\}$$

Here, $V(x)$ is the potential at location x, q is the elementary charge, ε_o is the vacuum permeability, n_o is the initial electron density near the cathode, α is the Townsend first ionization coefficient, and L is the gap size. It can be shown that provided that $\alpha L \gg 1$ (which is the case of interest when studying the rapid ignition of the discharge), the exponential profile captures the ion profile left behind by multiple simultaneous avalanches initiated by seed electrons regardless of whether these are concentrated near the cathode, uniformly distributed across the discharge gap, or distributed according to a cosine profile. This is so, because the contribution to the final density profile of the avalanche that starts near the cathode is much larger than any of the rest when $\alpha L \gg 1$.

Taking the cathode $(x = 0)$ as our reference electrode $V(0) = 0$, the solution of Poisson's equation yields

$$V^* = \frac{qn_o}{\alpha^2 \varepsilon_o} [1 + \alpha L \exp(\alpha L) - \exp(\alpha L)]$$
$$\text{with } \alpha \approx \alpha(V^*/L)$$
$$n^* = \frac{n_o}{\alpha L - 1} \left(\frac{V^* \alpha^2 \varepsilon_o}{q n_o} - 1 \right) \sim 10^{12} - 10^{13} \text{cm}^{-3}$$

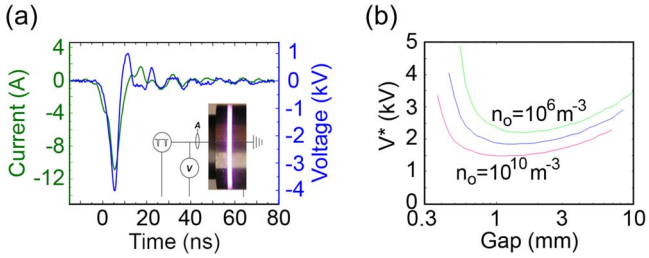

Fig. 9. (a) Voltage and current traces in a 10-ns discharge ignited with an average electric field of 4 kV/mm. (b) Voltage required to create a quasi-neutral plasma region without the contribution of secondary electrons as a function of the seed electron density.

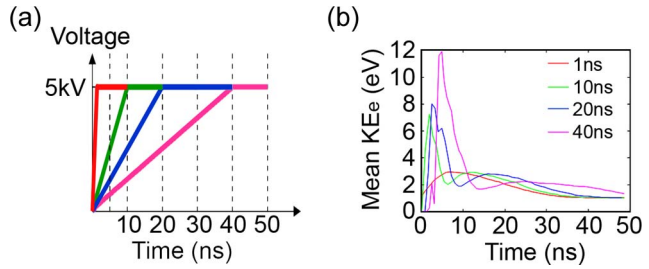

Fig. 10. Time evolution of the (a) applied voltage and (b) mean electron energy for nanosecond-pulsed discharges with pulses of different rise time.

where V^* and n^* are the critical voltage and the maximum density obtained when the avalanche initiated by seed electrons is just able to form a quasi-neutral plasma on the anode. If the applied voltage is smaller than V^*, the discharge is expected to ignite in the Townsend regime as shown in all the submicrosecond-pulsed atmospheric plasmas shown in the previous section. On the other hand, when the applied voltage is larger than V^*, the discharge is expected to ignite right after the application of the voltage pulse with no measurable delay between current and voltage traces [see Fig. 9(a)].

As shown in Fig. 9(b), where the aforementioned equation is plotted for helium at atmospheric pressure, the critical voltage for the transition into an instantaneous ignition depends on the number of seed electrons present in the gap from the previous pulse (n_o) and the gap size. A typical critical voltage of $V^* \sim 2$ kV is required for discharges with a ∼1-mm gap for the discharge to ignite instantaneously, and the density achieved right after the ignition is $n^* = 10^{12} - 10^{13}$ cm^{-3}. Submicrosecond-pulsed discharges shown in the previous section were sustained with $E = 0.5 - 1$ kV/mm $(E < V^*/d \sim 2$ kV/mm), whereas the discharge in Fig. 9(a) was ignited with $E = 4$ kV/mm $(E > V^*/d \sim 2$ kV/mm).

C. Study on the Pulse Rise Time

Control of the voltage waveform in a real device is quite challenging, and as a result, studies on the influence of different waveforms on the discharge characteristics are limited. These studies, however, can be addressed easily with computational models because the power source can be made ideal without the limitation of actual electronic devices. In this section, we study the characteristics of a discharge sustained with 5-kV pulses when the rise time is varied from 1 to 40 ns. The time evolution of the mean kinetic energy as a function of the rise time is shown in Fig. 10. As discussed earlier (Section III-C), the

maximum mean electron energy is achieved early on during the pulse, typically within 10 ns. The maximum kinetic energy is achieved with the pulse that has a rise time of 40 ns and not with the fastest rising time pulse. The reason for the smaller mean electron energy with the 1-ns rise-time pulse is due to the early formation of a quasi-neutral plasma as soon as the applied voltage increases above the critical value V^* ($\sim$2 kV for a 1-mm gap). When this happens, the electrons are shielded from the applied electric field, and although hot electrons will exist at the head of the cathode-directed ionization front, the mean electron energy of the whole electron ensemble reduces.

V. Conclusion

We have developed a hybrid model that is capable of modeling electron kinetics during the application of short intense pulses by means of a PIC-MCC approach while accounting for the discharge evolution during the pulse-off phase by means of a fluid model. This allows simulation to run for multiple pulses while treating electron kinetics accurately during the pulse-on phase. Simulation results have been compared with experimental data, and good qualitatively agreement is found among the two.

Experimental and computational results indicate that increasing the applied voltage results in faster ignition of the discharge and an increase in the mean electron energy. Therefore, it is, in principle, possible to tune the plasma chemistry to suit a given application by adjusting the pulse shape without having to change the physical configuration of the plasma source. Whereas submicrosecond-pulsed discharges are initiated by Townsend discharges in which the ignition is delayed with respect to the applied voltage, nanosecond-pulsed discharges ignite instantaneously without the involvement of secondary electrons. Despite the large pd values (30–300 torr $\cdot$ cm) and the high electric field (approximately kilovolts per millimeter), the discharges obtained remain in a glowlike mode and no streamers have been observed.

Finally, it is anticipated that pulsed discharges will offer the possibility of controlling the reactivity of low-temperature atmospheric-pressure plasmas by providing a better tunability of the electron energy than continuous wave discharges.

References

[1] F. Iza, G. J. Kim, S. M. Lee, J. K. Lee, J. L. Walsh, Y. T. Zhang, and M. G. Kong, "Microplasmas: Sources, particle kinetics, and biomedical applications," *Plasma Process. Polym.*, vol. 5, no. 4, pp. 322–344, Jun. 2008.

[2] K. H. Becker, K. H. Schoenbach, and J. G. Eden, "Microplasmas and applications," *J. Phys. D, Appl. Phys.*, vol. 39, no. 3, pp. R55–R70, Feb. 2006.

[3] Z. Cao, J. L. Walsh, and M. G. Kong, "Atmospheric plasma jet arrays in parallel electric and gas flow fields for 3D surface treatment," *Appl. Phys. Lett.*, vol. 94, no. 24, p. 021 501, Jan. 2009.

[4] R. J. Leiweke and B. N. Ganguly, "Effects of pulsed-excitation applied voltage rise time on argon metastable production efficiency in a high pressure dielectric barrier discharge," *Appl. Phys. Lett.*, vol. 90, no. 24, p. 241 501, Jun. 2007.

[5] M. Laroussi, "Nanoseconds pulsed non-equilibrium plasma discharges and applications," in *Proc. Int. Symp. Plasma Chem.*, Kyoto, Japan, 2007.

[6] G. L. Pilla, D. A. Lacoste, D. Veynante, and C. O. Laux, "Stabilization of a swirled propane–air flame using a nanosecond repetitively pulsed plasma," *IEEE Trans. Plasma Sci.*, vol. 36, no. 4, pp. 940–941, Aug. 2008.

[7] J. L. Walsh and M. G. Kong, "10 ns pulsed atmospheric air plasma for uniform treatment of polymeric surfaces," *Appl. Phys. Lett.*, vol. 91, no. 25, p. 251 504, Dec. 2007.

[8] J. L. Walsh, J. J. Shi, and M. G. Kong, "Submicrosecond pulsed atmospheric glow discharges sustained without dielectric barriers at kilohertz frequencies," *Appl. Phys. Lett.*, vol. 89, no. 16, p. 161 505, Oct. 2006.

[9] J. L. Walsh and M. G. Kong, "Sharp bursts of high-flux reactive species in submicrosecond atmospheric pressure glow discharges," *Appl. Phys. Lett.*, vol. 89, no. 23, p. 231 503, Dec. 2006.

[10] C. K. Birdsall and A. B. Langdon, *Plasma Physics via Computer Simulation*. Boca Raton, FL: CRC Press, 2004.

[11] H. C. Kim, F. Iza, S. S. Yang, M. Radmilovic-Radjenovic, and J. K. Lee, "Particle and fluid simulations of low-temperature plasma discharges: Benchmarks and kinetic effects," *J. Phys. D, Appl. Phys.*, vol. 38, no. 19, pp. R283–R301, Oct. 2005.

[12] F. Iza and J. K. Lee, "Moment conserving method for modelling multiple collisions in particle simulations," *J. Phys. D, Appl. Phys.*, vol. 39, no. 9, pp. 1853–1865, May 2006.

[13] F. Shi, D. Wang, and C. Ren, "Simulations of atmospheric pressure discharge in a high-voltage nanosecond pulse using the particle-in-cell Monte Carlo collision model in noble gases," *Phys. Plasmas*, vol. 15, no. 6, p. 063 503, Jun. 2008.

[14] F. Iza, J. K. Lee, and M. G. Kong, "Electron kinetics in radio-frequency atmospheric-pressure microplasmas," *Phys. Rev. Lett.*, vol. 99, no. 7, p. 075 004, Aug. 2007.

[15] J. P. Verboncoeur, M. V. Alves, V. Vahedi, and C. K. Birdsall, "Simultaneous potential and circuit solution for 1D bounded plasma particle simulation codes," *J. Comput. Phys.*, vol. 104, no. 2, pp. 321–328, Feb. 1993.

[16] M. Radmilovic-Radjenovic, J. K. Lee, F. Iza, and G. Y. Park, "Particle-in-cell simulation of gas breakdown in microgaps," *J. Phys. D, Appl. Phys.*, vol. 38, no. 6, pp. 950–954, Mar. 2005.

[17] M. A. Lieberman and A. J. Lichtenberg, *Principles of Plasma Discharges*, 2nd ed. Hoboken, NJ: Wiley, 2005.

[18] K. L. Cartwright, J. P. Verboncoeur, and C. K. Birdsall, "Loading and injection of Maxwellian distributions in particle simulations," *J. Comput. Phys.*, vol. 162, no. 2, pp. 483–513, Aug. 2000.

[19] Q. Wang, D. J. Economou, and V. M. Donnelly, "Simulation of a direct current microplasma discharge in helium at atmospheric pressure," *J. Appl. Phys.*, vol. 100, no. 2, p. 023 301, Jul. 2006.

[20] E. Wagenaars, M. D. Bowden, and G. M. W. Kroesen, "Measurements of electric-field strengths in ionization fronts during breakdown," *Phys. Rev. Lett.*, vol. 98, no. 7, p. 075 002, Feb. 2007.

[21] S. Li, J.-P. Lim, J. G. Kang, and H. S. Uhm, "Comparison of atmospheric-pressure helium and argon plasmas generated by capacitively coupled radio-frequency discharge," *Phys. Plasmas*, vol. 13, no. 9, p. 093 503, Sep. 2006.

[22] E. Stoffels, A. J. Flikweert, W. W. Stoffels, and G. M. W. Kroesen, "Plasma needle: A non-destructive atmospheric plasma source for fine surface treatment of (bio)materials," *Plasma Sources Sci. Technol.*, vol. 11, no. 4, pp. 383–388, Nov. 2002.

[23] M. Ishimaru, T. Ohba, T. Ohmori, T. Yagisawa, T. Kitajima, and T. Makabe, "Diagnostics for low-energy electrons in a two-frequency capacitively coupled plasma in Ar," *Appl. Phys. Lett.*, vol. 92, no. 7, p. 071 501, Feb. 2008.

[24] L. B. Loeb and J. M. Meek, "The mechanism of spark discharge in air at atmospheric pressure. I," *J. Appl. Phys.*, vol. 11, no. 6, pp. 438–447, Jun. 1940.

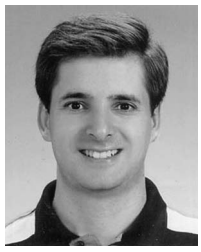

Felipe Iza (S'03–M'05) received the B.S. degree in engineering from the University of Navarra, San Sebastian, Spain, in 1997, and the M.S. and Ph.D. degrees from the Northeastern University, Boston, MA, in 2001 and 2004, respectively.

From 1997 to 1999, he was with the Centro de Estudios e Investigaciones Tecnicas de Guipuzcoa, San Sebastian. From 2004 to 2006, he was a Postdoctoral Fellow with Pohang University of Science and Technology, Pohang, Korea, where he became a Research Professor in 2006. Since 2007, he has been a Lecturer with the Department of Electronic and Electrical Engineering, Loughborough University, Leicestershire, U.K. His research interest is focused on experimental and computational low-temperature plasmas with special attention to microplasmas and atmospheric discharges for biomedical applications.

Dr. Iza is a Fulbright alumnus and a member of the American Vacuum Society.

James L. Walsh received the M.Eng. degree in systems engineering and the Ph.D. degree in electrical engineering from the Loughborough University, Leicestershire, U.K., in 2004 and 2008, respectively.

Since 2006, he has been a Research Associate with the Plasma & Pulsed Power Group, Department of Electronic and Electrical Engineering, Loughborough University. His current research interests include very high frequency radio-frequency discharges and nanosecond-pulsed plasmas.

Michael G. Kong (M'94–SM'98) received the B.Sc. and M.Sc. degrees in electronics from Zhejiang University, Hangzhou, China, and the Ph.D. degree in electrical engineering from the University of Liverpool, Liverpool, U.K.

After research and teaching posts at the University of Nottingham, Nottingham, U.K., and University of Liverpool, he joined Loughborough University, Leicestershire, U.K., in 1999, where he is currently a Chair in bioelectrical engineering with the Department of Electronic and Electrical Engineering. He is a Cofounder of a $5M Centre for Biological Engineering at Loughborough University. His research interests include nonthermal atmospheric discharges and electromagnetic fields as well as their applications to medicine and biology.

Dr. Kong was a Guest Editor for a special issue of the IEEE TRANSACTIONS ON PLASMA SCIENCE (Nonthermal Biomedical Applications of Ionizing Gases and Electromagnetic Fields, August 2006).